Journal of Structural Geology, Vol. 12, No. 4, pp. 499 to 512, 1990
Printed in Great Britain

0191-8141/90 $03.00+0.00

Extensional duplexing in the York Cliffs strike-slip fault system, southern coastal Maine

MARK T. SWANSON

Department of Geosciences, University of Southern Maine, Gorham, ME 04038, U.S.A.

(*Received* 11 *October* 1988; *accepted in revised form* 28 *November* 1989)

Abstract—A 150 m-long sinistral strike-slip fault system, consisting of left-stepping en échelon fault segments, cuts deformed Paleozoic metasediments and early Mesozoic dike intrusions in coastal terrace outcrops in southern Maine. The longer fault segments follow the vertical bedding in the metasediments and accommodate approximately 1 m of displacement. Detailed mapping at scales down to 1:6, indicates that overlap zones between offset layer-parallel fault segments consist of high-dilation angular breccias, rounded attrition breccias and extensional duplexes where the offset segments straddle upright quartzite layers.

In one 10 m-long duplex, *R*- and *R'*-shears cut the layering in the quartzite at 28° and 69°, respectively, relative to the dominant layer-parallel fault segments, creating a doubly-tapered imbricate *R*-shear lens segmentation structure. Individual imbricate lenses accommodate additional layer-parallel extension through conjugate *X*–*X'*-shear fractures with average orientations of 109° and 60°, respectively, relative to the dominant fault segments. Extensional fractures oblique to the dominant fault segments are rare within this duplex but commonly form distinctive 'horsetail' arrays at fault terminations that average 44° to the layer-parallel faults. Strain analysis shows that approximately 60–80 cm of measured strike-slip displacement is accommodated internally within this duplex as layer-parallel extensional strain using the *R*-shear and *X*–*X'*-shear fracture mechanisms. The strain distribution and observed cross-cutting relations suggest an outward symmetric growth of the duplex structure from left-stepping, sinistral fault segments that developed sequences of tip-to-plane *R*-shear overlap linkages during continued displacements. Cyclic *R*–*R'*- to *X*–*X'*-shear fracturing may relate to stress reorientation following *R*-shear ruptures during episodic growth of the duplex and incremental slip of the fault system.

INTRODUCTION

FAULT zone evolution typically involves the initiation of a system of en échelon fault segments that link together to form a through-going structure. Left-stepping offsets between sinistral en échelon fault segments, as discussed in this paper, call for extension of the bridge areas or offset–overlap zones between faults during linkage. The style of such extensional linkage (Fig. 1) involves the formation of dilation breccias and mineral-filled voids, attrition breccias and gouge layers as well as fault duplexes within the offset–overlap zones. The duplex style of extensional linkage will be the main focus of this paper.

Duplex terminology in thrust zones (Dahlstrom 1970, Boyer & Elliot 1982) has been expanded to the normal fault (Gibbs 1984) as well as to the strike-slip fault (Woodcock & Fischer 1986) regimes. Duplexes in en échelon strike-slip faults are characterized as extensional (Fig. 2a) or contractional (Fig. 2b) depending on the stepping direction, sense of slip and the nature of the internal deformation. Duplexing in the strike-slip, as opposed to the thrust, environment also typically develops a braided disorganized geometry in the absence of a controlling planar anisotropy such as bedding (Woodcock & Fischer 1986).

This paper addresses a small-scale sinistral strike-slip fault in southern coastal Maine in the northeast U.S. that formed sub-parallel to a prominent vertical bedding-anisotropy in the limbs of upright Paleozoic folds (Swanson 1987). This bedding anisotropy exerts a strong influence on rupture geometry resulting in dis-

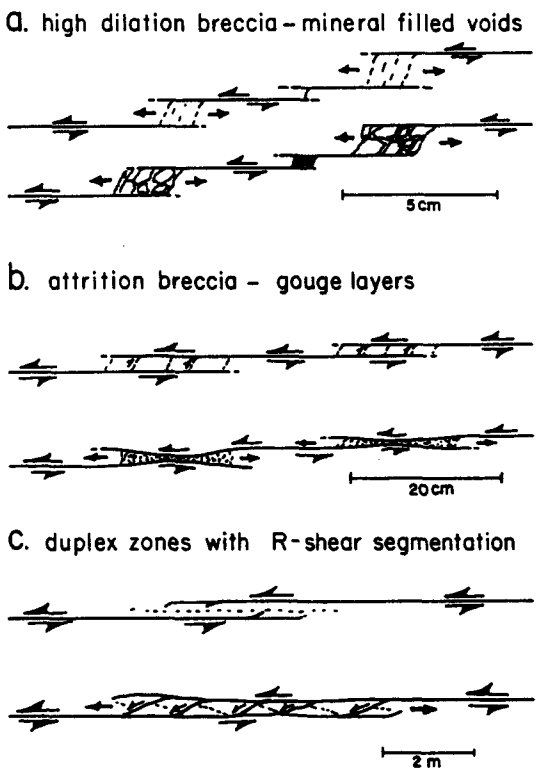

Fig. 1. Types of extensional linkages between en échelon fault segments: (a) high dilation breccias with angular fragments and wall-supported open-cavity mineralization; (b) attrition breccia, microbreccia and gouge layers due to disruption, rotation and comminution of the intervening host rock showing distinctive stretching and thinning related to fault-parallel extension; and (c) duplex zones with *R*-shear segmentation.

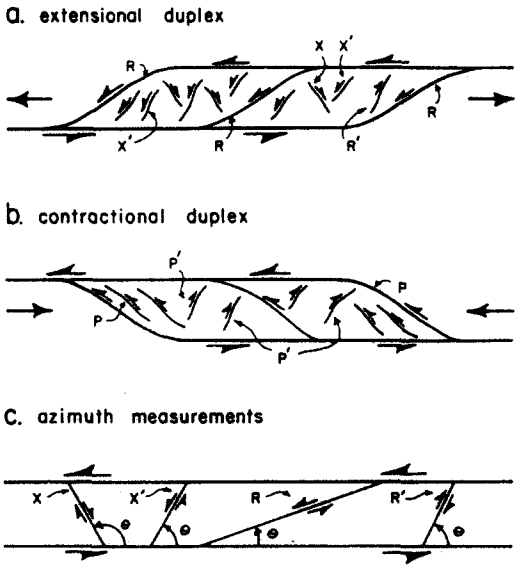

Fig. 2. Geometry of offset–overlapping ends of en échelon strike-slip fault segments showing the nature of the internal strain and shear fracture terminology used in the text: (a) extensional; (b) contractional duplexes; and (c) orientations of dominant fracture sets measured counterclockwise relative to bedding-parallel fault segments.

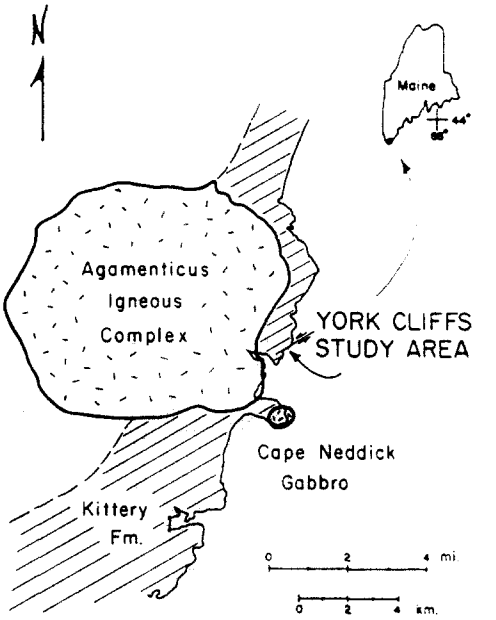

Fig. 3. Local geologic setting and field study location in coastal exposures of southern Maine (after Hussey 1962, Swanson 1982).

tinctive, elongate duplexes where overlapping fault segments straddle competent quartzite layers. Detailed fault maps were drawn from photomosaics at a scale of 1:6. Displacement, orientation, bed-length and area measurements are used to estimate strain distributions in this duplex and reconstruct the kinematic development of the fault system. An understanding of the deformation mechanisms within stepover zones or jog areas between en échelon fault segments is important to the study of earthquake faulting, since large-scale earthquake ruptures appear to attenuate at dilational fault jogs (Sibson 1985).

GEOLOGIC SETTING

The Precambrian–Ordovician (?) Kittery Formation (Hussey 1962) of southern coastal Maine (Fig. 3) consists of a turbiditic sequence of quartzites and pelitic schists. This sequence was deformed by early F_1 recumbent folds and later upright, gently-plunging, open to isoclinal F_2 folds of probable Paleozoic age. Tight F_2 folds create a prominent NE-trending vertical bedding-anisotropy in the York Cliffs exposures. Later Mesozoic extension led to the development of the Agamenticus alkaline complex of early Triassic age, a NE-trending mafic dike swarm complex of largely early Jurassic age, and the Cape Neddick gabbroic complex of Cretaceous age (Fig. 3).

Localized extensional fractures and minor strike-slip faults with quartz and calcite mineralization are common within these coastal exposures (Swanson 1982) and are generally associated with the later phases of the Jurassic dike intrusion. The strike-slip fault system at York Cliffs is sinistral, with up to ~1.4 m offset of early quartz veins and mafic to felsic dike segments. The Jurassic or younger age of faulting and probable rates of Mesozoic and Cenozoic erosion (Doherty & Lyons 1980) suggest the mapped faults formed at depths of ~5 km and ambient host rock temperatures of ~170°C.

YORK CLIFFS FAULT SYSTEM

The sinistral strike-slip fault system at York Cliffs (Fig. 4) is ~150 m long from termination to termination. The dominant fault segments trend 055° and have a generally steep 85°NW dip (Fig. 5), sub-parallel to bedding in the host Kittery Formation. The dominant fault segments often consist of several layer-parallel slip surfaces generally concentrating in the pelitic interbeds flanking more competent quartzite beds. The high-angle orientation of the shear and extension fractures (85° dip) and minor sub-horizontal striations (16° plunge to 254°) indicate plane strain and attest to the dominantly strike-slip nature of the brittle structures. Thus measured strike-separations on the map are a good approximation to actual strike-slip displacements.

Structural data (Fig. 5a) distinguishes between various sets of both dextral and sinistral faults relative to the layer-parallel duplex boundaries. Angular relationships of minor shears with respect to the dominant slip surface are measured counterclockwise (Fig. 2c) from the reference layer-parallel fault surface that strikes ~055°. The shear fracture terminology (Figs. 2 and 5a) used in this report is that of Logan *et al.* (1979) and Swanson (1987, 1988). Fractures were assigned to a specific group depending on the orientation and sense of slip. The overall geometry of the fault system, as described by poles to the dominant measured fracture surfaces, is reflected in a nearly horizontal movement plane with a corresponding steeply-plunging (Fig. 5b) kinematic rotation pole that

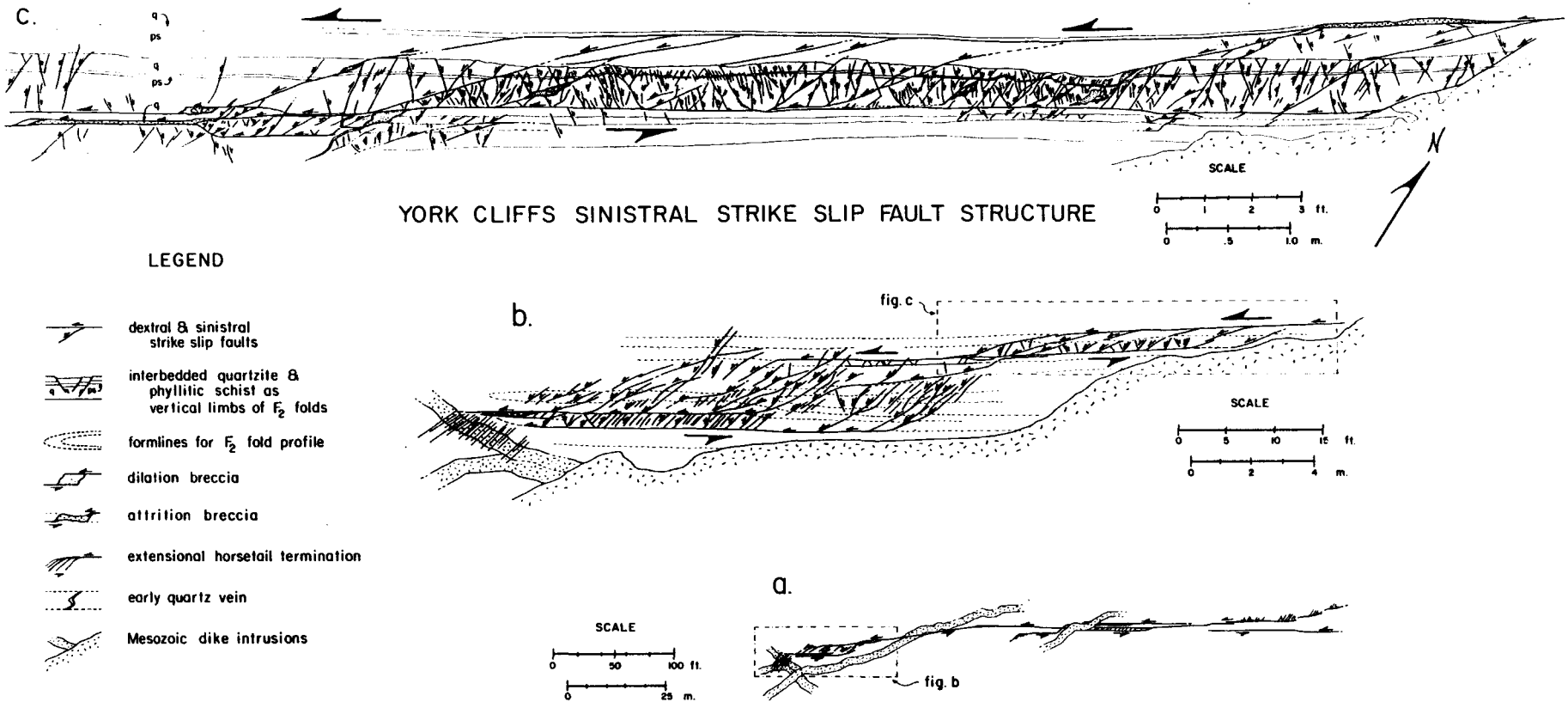

Fig. 4. The York Cliffs sinistral strike-slip fault system: (a) reduced version of original 1:240 field scale sketch map of the entire York Cliffs fault system; (b) reduced version of original 1:60 field scale map of the southwest termination; and (c) reduced version of original 1:6 field-scale map of the quartzite-slab duplex.

approximates the intermediate principal stress axis for this essentially strike-slip deformation. The entire fault is exposed and measured displacements vary from zero at the terminations, to 0.8 m at the southwest duplex, to 1.0–1.2 m through the cross-cut Mesozoic dikes, to a maximum of 1.38 m in the mid-section corresponding to a maximum displacement/length ratio (D_{max}/L), after Muraoka & Kamata (1983), of ~0.01.

The overall structure (Fig. 4) consists of a series of thin, elongate and generally extensional, duplexes that form in competent quartzite layers along the main fault surfaces. These duplexes form the left-stepping offset zones between en échelon sinistral fault segments that parallel vertical bedding in the Kittery Formation. The left-stepping nature of the segments leads to the dominant extensional nature of the associated duplexes, which are particularly well-developed where the segments step across competent quartzite units (Fig. 4a). Details of the style of deformation within the offset–overlap zones between the ends of en échelon fault segments are superbly exposed. Oblique extensional fracture arrays, in 'horsetail' termination configurations (Granier 1985) similar to feather fractures of Friedman & Logan (1970), mark both ends of the exposed fault system (Fig. 4b & c).

The fault system's southwest termination (Fig. 4b) coincides with the competent hinge zone of a gently-plunging isoclinal fold. This termination consists of a series of generally extensional, but minor contractional, duplex-type linkages. A 6 × 30 m extensional duplex links two left-stepping fault segments as they step across the vertical bedding. Linking faults are dominated by sinistral X'-shear or composite R–X'–R-shear fractures. A smaller (3 × 0.5 m) contractional duplex with a distinctive dextral shear array at high-angles to the dominant fault segment formed along the southeast side of the termination. The two structures converge along a 10 cm wide dilational breccia zone with intense extensional fracturing at the horsetail termination.

The main extensional linkage (Fig. 4b) also contains a distinctive smaller duplex, 10 m in length, developed about a 0.5 m thick quartzite layer (Figs. 4b & c). The quartzite layer is flanked to the northwest by less competent pelitic schists and to the southeast by sinistral slip surfaces parallel to bedding. Discrete sinistral R-shear surfaces, that cut the pelitic schists, distribute the displacement and cut into the adjoining quartzite layer. The internal structure of the quartzite duplex consists of a series of R-shears at low-angles to the layer-parallel bounding faults. These R-shears form the end ramps to the duplex and divide the quartzite slab into double-tapered imbricate lenses where each lens suffered additional layer-parallel extension through internal X–X'-shear fracturing and minor brecciation. This extensional duplex also has a smaller contractional ramp and slab (0.5 × 0.1 m) associated with it along its southeast flank in a configuration similar to the larger contractional duplex slab described above.

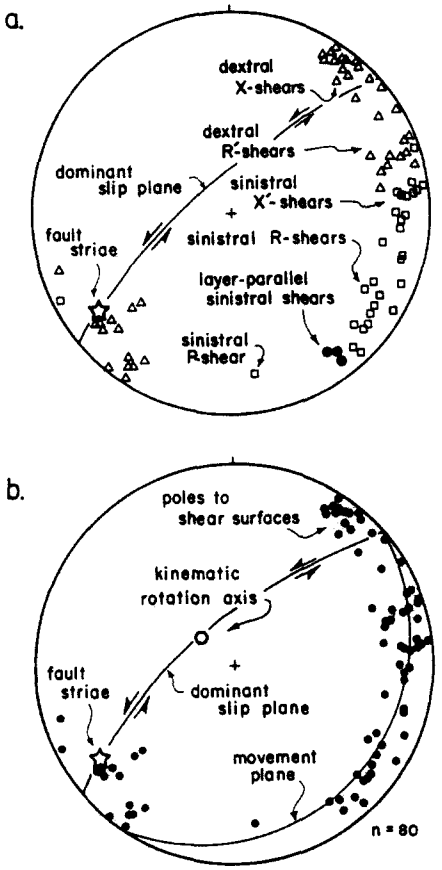

Fig. 5. Stereonet representation of fault orientations within quartzite-slab duplex: (a) poles to measured shear fracture orientations with trace of dominant slip plane and plunge of fault striae; (b) best-fit great circle for shear fracture orientations in (a) above representing movement plane with corresponding kinematic rotation pole that approximates the intermediate stress orientation. Trace of dominant slip plane and plunge of fault striae also indicated.

BRECCIA DEVELOPMENT

The types of extensional linkages developed between en échelon layer-parallel fault segments observed in these exposures (Fig. 1) include the above duplexes and, on a somewhat smaller scale, localized fault breccias. Fault breccias of two different types form a distinctive component of the York Cliffs fault system (see Fig. 4c), which occur in small rhombohedral pull-apart zones at bends and offsets along faults (dilational breccias) and as thin layers of disrupted quartzite (attrition breccias) along the fault segments.

Dilation breccias

The dilation breccias (Fig. 1a) consist of medium- to coarse-grained angular quartzite fragments cemented by calcite, quartz and muscovite developed at small-scale extensional step-over zones and releasing bends or jogs along minor shear fractures within competent layers. These breccias are equivalent to the dilation breccias of Sibson (1986). Fault-parallel dilation produces rhombohedral pull-aparts that accommodate the strike-slip displacement. Open cavity mineralization suggests void spaces are supported by competent wall rocks during dilation.

Attrition breccias

The attrition breccias (Fig. 1b) occur as disrupted quartzite layers developed along thin, isolated, cm-thick quartzite layers within dominantly pelitic host rock. These breccias are actually small-scale examples of extensional duplexes where the disrupted quartzite layers are bound by slip surfaces at contacts with surrounding pelitic schist units. The breccias vary from minor coarse-grained varieties that represent the initial disruption of the layers to medium- and fine-grained varieties, as breccia, microbreccia and gouge. The incompetent wall rocks prevent the formation of significant open cavity mineralization due to dilation. Layer-parallel extension results in significant thinning and stretching of the disrupted layer. These disrupted quartzite layers are similar to the attrition breccias of Sibson (1986) where brecciation develops by the rotation, abrasion and comminution of initially angular quartzite fragments. Layer-parallel extension of stretched and thinned disrupted quartzite layers in these breccias is used to estimate displacements on the adjoining fault segments.

The initial fracturing and counterclockwise rotation involved in the disruption and fragmentation of a thin 4 cm thick quartzite layer is depicted in Fig. 6. Farther along strike from this disrupted zone, the layer has suffered extreme thinning and comminution, forming a layer of microbreccia and gouge down to essentially zero thickness. The 25° of counterclockwise rotation of the larger disrupted fragments in this example is based on the orientation of layering within the breccia fragments and accompanies sinistral displacement with dextral slip and rotation of the intervening shear fracture surfaces. The angles between the quartzite fragment boundaries (as the initial fracture surface) and the layering within the fragments indicate the fracture orientations at the time of disruption, which vary from 50° to 74° relative to the layer-parallel reference surface. These fractures may have initiated as tension fractures at angles close to 45° from the layer-parallel fault surface with subsequent counterclockwise rotation and reactivation in dextral shear *and* as minor early dextral R'-shears at approximately 70° to the fault-parallel layering. A similar process of initial disruption developed along the larger contractional slab (Fig. 4b) with its prominent high-

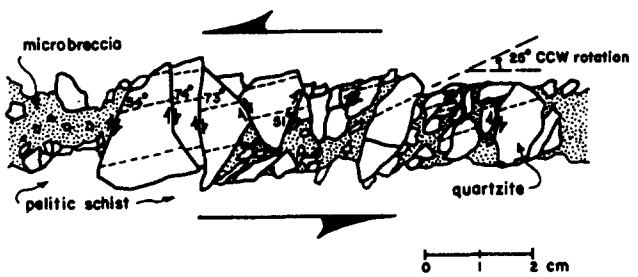

Fig. 6. Disruption of quartzite layer by dextral R'-shear fractures and reactivated extension fractures (initial 51–74° orientations relative to bedding in clasts) with the counterclockwise (CCW) rotation (25°) of fragments, as measured from the reoriented remnant bedding in the quartzite, leading to the development of attrition breccia, microbreccia and gouge.

angle dextral (antithetic) shear array and slight (8°) counterclockwise rotation of quartzite blocks and intervening fractures. Most of these dextral shears represent reactivated oblique tensional fractures with only a few as true R'- shears. This suggests that sets of oblique tension fractures reactivated under dextral shear and minor R'-shears were responsible for the initial disruption of the quartzite layer through counterclockwise clast rotation during displacement. This compares favorably with the oblique tensional fracturing mechanism invoked by Engelder (1974) for the initiation of cataclasis and the generation of fault gouge as well as the forward-rotating fracture mechanism of Hanmer (1989) for the initiation of cataclastic flow.

INTERNAL DUPLEX GEOMETRY

Internal deformation within the quartzite-slab duplex (Fig. 4c) was accommodated by sets of R–R' and X–X'-shear fractures (after Logan *et al.* 1979, Swanson 1988). As illustrated in Fig. 7(a) the dominant R-shears within the duplex segment the quartzite layer into imbricate lenses. Deformation within these doubly-tapered lenses was accommodated by minor R'-shear fractures and a conjugate set of X–X'-shear fractures (Fig. 7b). The internal deformation varies from minimal fragmentation to total disruption, with local calcite–quartz cemented breccias.

The X–X'-shear fractures (Fig. 7b) are the most abundant subsidiary fractures developed within this duplex representing 53% and 22%, respectively, of the 380 measured shear fractures (Fig. 8a). The R–R'-shear fractures are the least abundant with 5% and 20%, respectively (Fig. 8a). The orientations for these shear fracture sets (Figs. 8b & c) were measured counterclockwise from the layer-parallel slip surfaces that define the duplex boundaries. Average orientations for the different shear fracture sets are 28° (R), 69° (R'); 60° (X') and 109°(X), but these values include the effects of fault rotation subsequent to initiation, as discussed below.

The dextral shear fracture histogram (Fig. 8b) includes the X- and R'-shear fractures representing separate orientation peaks. The X-shear fracture peak consists of a primary maximum at approximately 105° that likely represents the angle of initiation. The asymmetric tail and secondary maximum at 125° are the result of counterclockwise rotation of these minor faults during displacement. The R'-shear fracture peak near 70° represents shear fractures related to the R-shear segment boundaries as conjugate sets of R–R'-shear fractures developed during simple shear.

The sinistral shear fracture histogram (Fig. 8c) includes the X'- and R-shear fractures in a composite asymmetric distribution. The asymmetric tail in this histogram is skewed toward the lower angle orientations and represents minor but prominent R-shears that accommodate most of the deformation. The remaining portion of this histogram consists of two obvious maxima

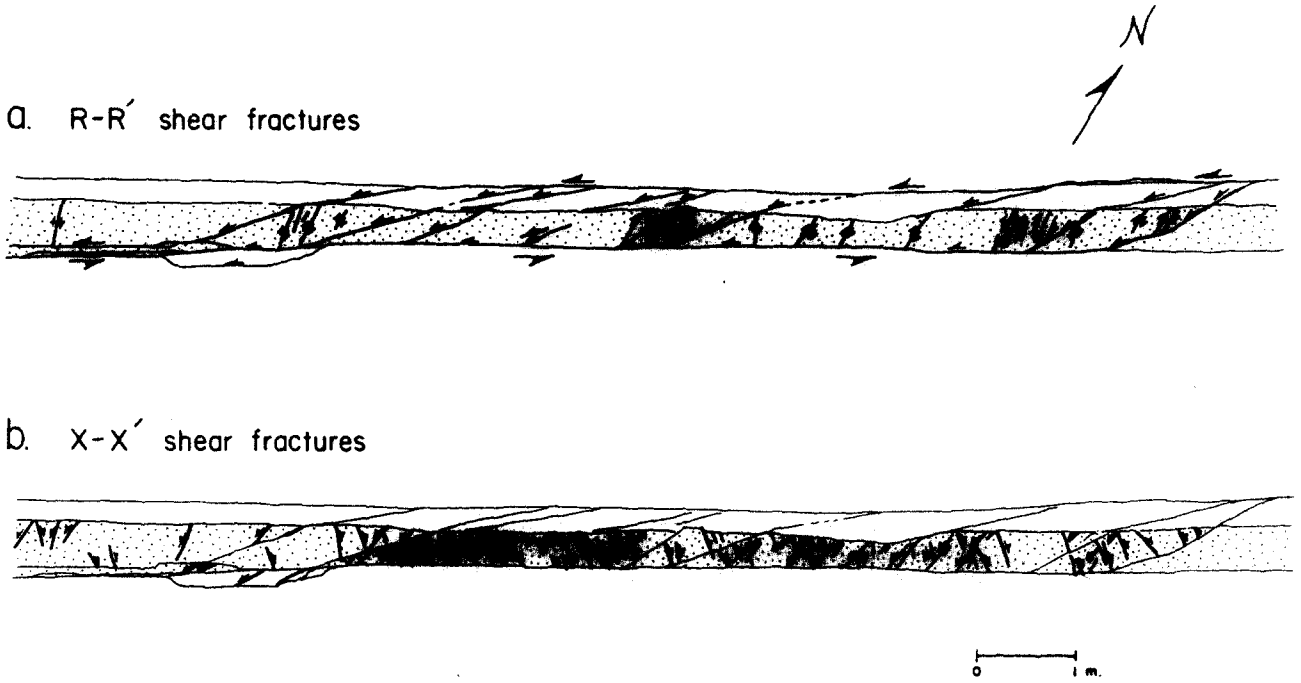

Fig. 7. Internal geometry of the quartzite-slab duplex of Fig. 4(c) showing the distribution of conjugate shear fractures: (a) *R*–*R'*-shear fractures; and (b) *X*–*X'*-shear fractures.

at approximately 55° and 75°. The more dominant peak at 55° represents the *X'*-shear fractures, most likely initiated near 75° with clockwise rotation to lower angles during displacement. The relatively small 30° dihedral angle for the *X*–*X'*-shear fracture set suggests tensional or near-tensional conditions associated with the dominantly brittle faulting.

KINEMATICS

The extensional duplex in Fig. 4(c) was segmented by prominent *R*-shears into asymmetric, doubly-tapered, imbricate lenses, labeled B–H in Fig. 9. Zone A is host rock outside of the end ramps to the duplex. Estimates of the bulk layer-parallel extension and overall fault displacements are derived by several techniques. This allows the contributions of the various fracture sets in accommodating displacements to be assessed and the strain distribution within the duplex to be evaluated. The bulk strain estimates are, then, an adequate basis for kinematic modelling.

Using mapped orientations and measured strike-separations (that approximate displacements) of 380 individual fractures, I calculated the bulk layer-parallel extension due to faulting by several techniques summarized in Fig. 10. These techniques included an orientation–displacement method, a bed-length reconstruction and a bed-thickness reconstruction for establishing the changes in length of the quartzite slab due to fault-parallel extension associated with sinistral layer-parallel displacement along the fault.

Total layer-parallel extensional strain was calculated as 8% by the orientation-displacement method, 10% by the bed-length reconstruction method and 14% by the initial bed thickness method. Using a final measured bed-parallel duplex length of approximately 9.4 m, these extension values correspond to equivalent layer-parallel displacements of approximately 65, 80 and 110 cm, respectively, along the layer-parallel fault segments. It is the higher values that are considered more accurate as the initial bed thickness reconstruction probably accounts for most of the deformation mechanisms on both the meso- and micro-scales.

Layer-parallel displacements can be measured directly in the field but good cross-strike markers are rare in the immediate vicinity of this duplex. In many places the dominant fault segment consists of several layer-parallel slip surfaces generally concentrating strain in the more pelitic interbeds. A nearby displaced Mesozoic dike margin suggests approximately 1 m of slip going southwest towards the duplex. Oblique *R*-shears within the immediately adjacent pelitic schist unit suggest approximately 82 cm of displacement along the outer northwest boundary zone of the duplex, although not all of this displacement may have been transferred into the adjacent quartzite unit. Incremental displacements along shear fractures within the quartzite yield 63 cm of sinistral displacement, but many of the smallest shear fractures, with displacements of less than a mm, and small areas of dilation breccia were neglected in the analysis. Strain estimates using the initial bed thickness reconstruction for a small layer-parallel attrition breccia zone (neglecting any volume occupied by mineralization) are at 94% extension and represent 64 cm of displacement transferred through this zone.

Using the lower 65 cm displacement derived from the orientation–displacement method as an average value, the dominant *R*-shears can account for nearly 60% of the transferred displacement. The internal shear fractures,

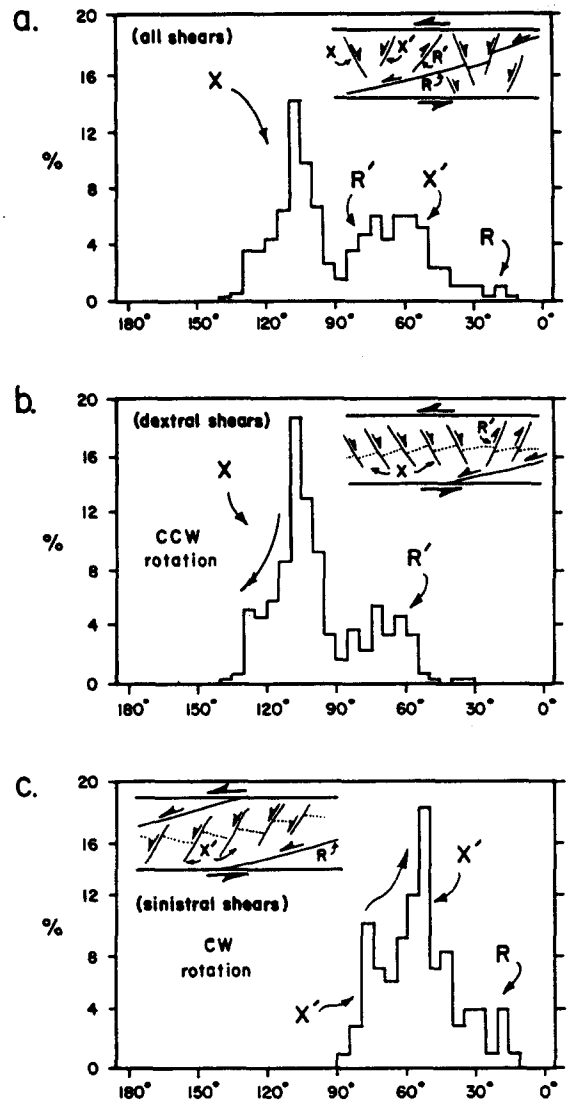

Fig. 8. Histograms of shear fracture azimuths measured counterclockwise from the layer-parallel fault segments: (a) composite histogram of all shear fractures (R, R', X, X') showing orientations and relative abundances; (b) dextral shear fracture histogram (R', X) showing orientations with skewed distributions due to counterclockwise (CCW) rotation during slip; and (c) sinistral shear fracture histogram (R, X') showing orientations with skewed distributions due to clockwise (CW) rotation during slip.

mainly X–X'-shears, accommodate an additional 40% of the transferred displacement. Higher 82 cm displacement values measured from shears in the adjacent pelitic schists require that the R-shear and X–X'-shears each accommodate approximately 50% of the extension in the duplex. The orientation–displacement method also indicates that the X-shear fractures accommodated 53% of the extensional strain, whereas the X'-shear fractures accommodated only 29%. Minor internal R-shears within the doubly-tapered imbricate lenses, not the lens boundaries themselves, only accounted for 6% of the strain. The R'-shears within the lenses contributed a negative 12% as shortening included in the total effective layer-parallel extension values.

The distribution of strain *within* the doubly-tapered, imbricate lens zones was also estimated using the orientation–displacement as well as the bed-length reconstruction methods. Results are similar for the two methods. Calculated bulk strains (Fig. 9) by the orientation–displacement method ranged from a fraction of a percent outside the duplex (zone A) and at the end zones (B and H) to maxima of 6–9% within internal zones C, D and F. The strain estimates for zones D and F are minimum values because the intense faulting in these zones is not completely accounted for in this analysis. The highest strain values obtained by the bed-length reconstruction method are 9% and 14% for internal zones D and F. These strain values correlate (Fig. 9) with fracture data within the imbricate R-shear lenses, such as, total number of fractures, total fracture length, fracture density (as the number of fractures per square meter) and accumulated displacements. This suggests a bimodal distribution of maximum strain along the length of the duplex concentrated in lens zones D and F.

DUPLEX GROWTH

The growth and development of the York Cliffs duplex is reconstructed from the mapped fault–fracture patterns (Fig. 4), measured displacements, observed cross-cutting relations and estimated strain distributions (Fig. 9). The hypothesized initial sinistral strike-slip faults probably consisted of several left-stepping en échelon segments, 5–30 m in length. Offsets between fault segments are from 0.5 to 2.0 m, with fault segment overlap up to ~20 m. Some of the initial segments may have developed with only 1 or 2 m of overlap before the onset of mechanical interaction and the formation of linkage structures. These linkage structures evolve as extensional duplexes that grow during continued displacements.

Larger duplex linkage at southwest termination

The larger duplex linkage structure at the southwest termination is thought to have developed from the initial offset and slightly overlapping left-stepping fault segments in Fig. 11(a). Outward growth of this extensional linkage proceeded through distributed X'-shear fracturing (Fig. 11b) in the offset–overlap zone that linked to the dominant fault surfaces along low-angle R-shears. R-shear segmentation is not developed here due to the lack of distinct lithologic control and the width of the initial en échelon offset. An additional phase of duplex growth (Fig. 11c) involved the formation of the larger contractional slab with its high-angle dextral shear array. This layer-parallel slip surface is linked to the opposing en échelon segment through an X'-shear fracture array and an R-shear ramp. The orientation–displacement method indicates ~4% layer-parallel shortening in this contractional duplex. Thus an additional 20 cm of slip was transferred through this structure. This sequence suggests growth of the duplex structure first to the southwest followed by a phase of growth to the northeast of the initial overlap.

The larger contractional slab may have developed as a consequence of the pattern of linkage between the two

STRAIN & FRACTURE DATA

ZONE		A	B	C	D	E	F	G	H
layer-parallel extension,%	(o.d.)	0.2	0.1	9.1	6.1	1.4	5.0	1.2	0.1
	(b.l.)	0.9	0.9	5.9	8.5	4.2	14.1	1.8	1.2
no. of fractures		14	14	44	109	15	97	56	17
total fracture length (cm.)		400	250	460	1200	230	1000	690	220
fractures/sq. meter		15	40	290	240	95	240	140	95

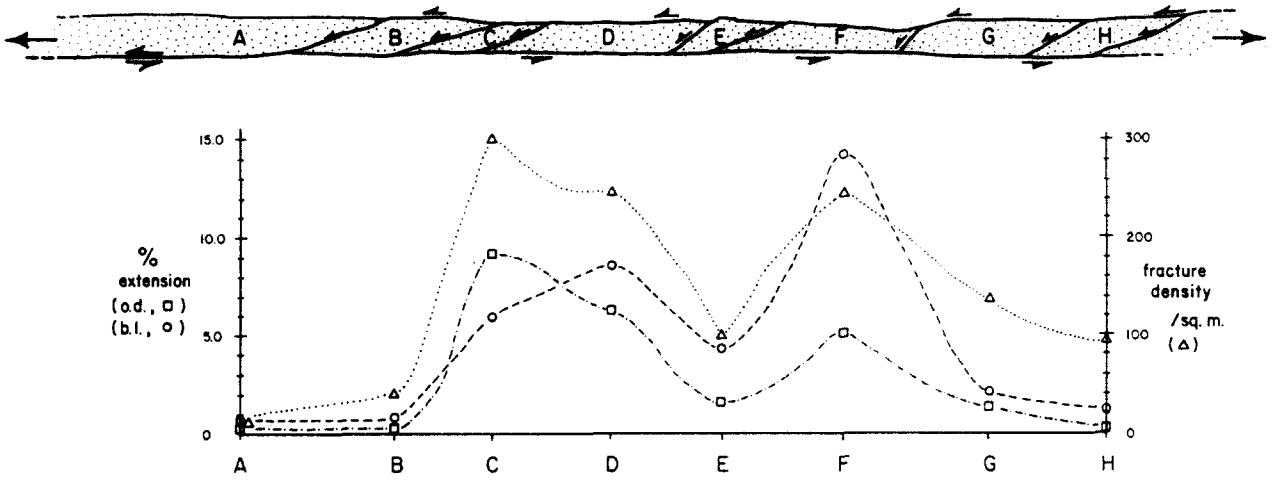

Fig. 9. Distribution of calculated extensional strains and fracture data for segmented lenses within the quartzite-slab duplex of Fig. 4(c). Layer-parallel extensional strain data utilized the orientation–displacement (o.d.) and the bed-length reconstruction (b.l.) techniques.

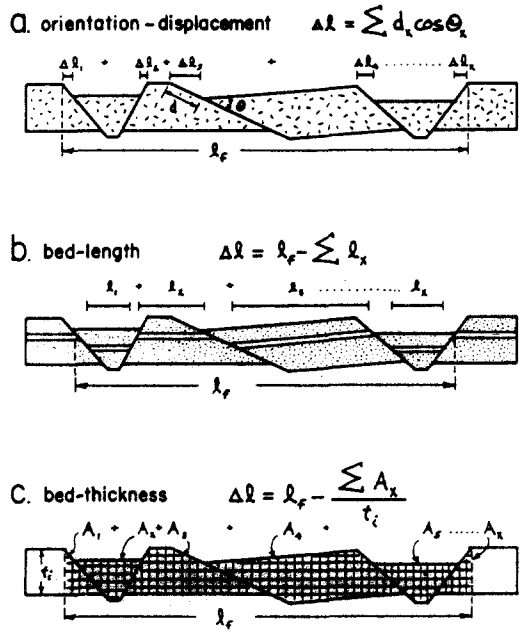

Fig. 10. Summary of techniques used to estimate changes in length of the quartzite slab for determination of layer-parallel extensional strain: (a) orientation–displacement method calculates contribution of each fault to layer-parallel extension due to slip; (b) bed-length reconstruction calculates the initial slab length by measuring individual bed segments between faults; and (c) bed-thickness reconstruction uses planimeter measurements of subareas within segmented slab for total area that is redistributed to initial slab thickness. In all cases, the change in length approximates displacement transferred through the duplex structure.

en échelon strike-slip segments. The second phase linkage propagation, to the southwest, could have overshot the position of the adjoining en échelon segment, thereby decoupling a section of anisotropy outboard of the offset–overlap zone. The propagating layer-parallel shear fracture would have had to ramp back to the proper horizon in order to complete the linkage. This realignment is accommodated by the leading *P*-shear ramp structures and internal shortening within the decoupled slab along a set of reactivated oblique extensional fractures and minor *R'*-shears.

Smaller quartzite-slab duplex

The initial rupture configuration for the quartzite-slab duplex (Fig. 12) apparently required only about 1 m of overlap before a tip-to-plane type of mechanical interaction resulted in the isolation of the central segment, zone E, and the development of its internal *X–X'* extension. The distribution of layer-parallel extension within the segmented duplex (Fig. 12) indicates two centrally-located maxima (zones D and F). This distribution of maximum extension into a pair of internal zones is similar to the double-basin pull-apart model of Hempton & Neher (1986) and reflects the overlap tip-to-plane fault interactions. The progressive decrease in extension outward from the central zones also suggests an outward expansion of the duplex during growth and

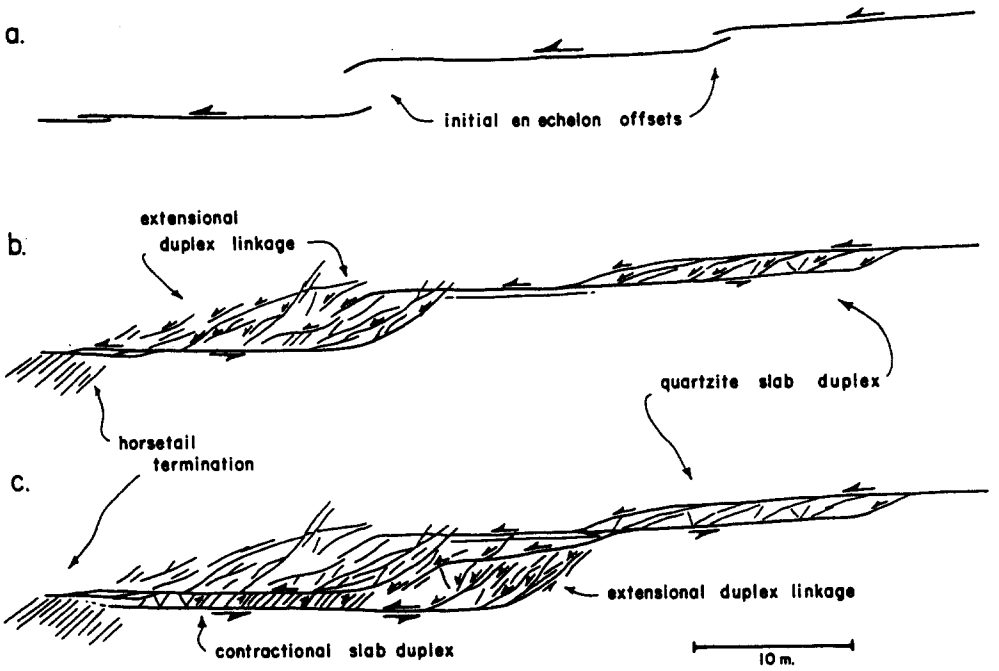

Fig. 11. Hypothesized initial en échelon fault array and developmental sequence for the southwest termination in the Fig. 4(b) fault map: (a) initial offset en échelon fault segments; (b) formation of the extensional duplex linkage and the horsetail termination array; and (c) further growth of the extensional linkage and formation of contractional slab.

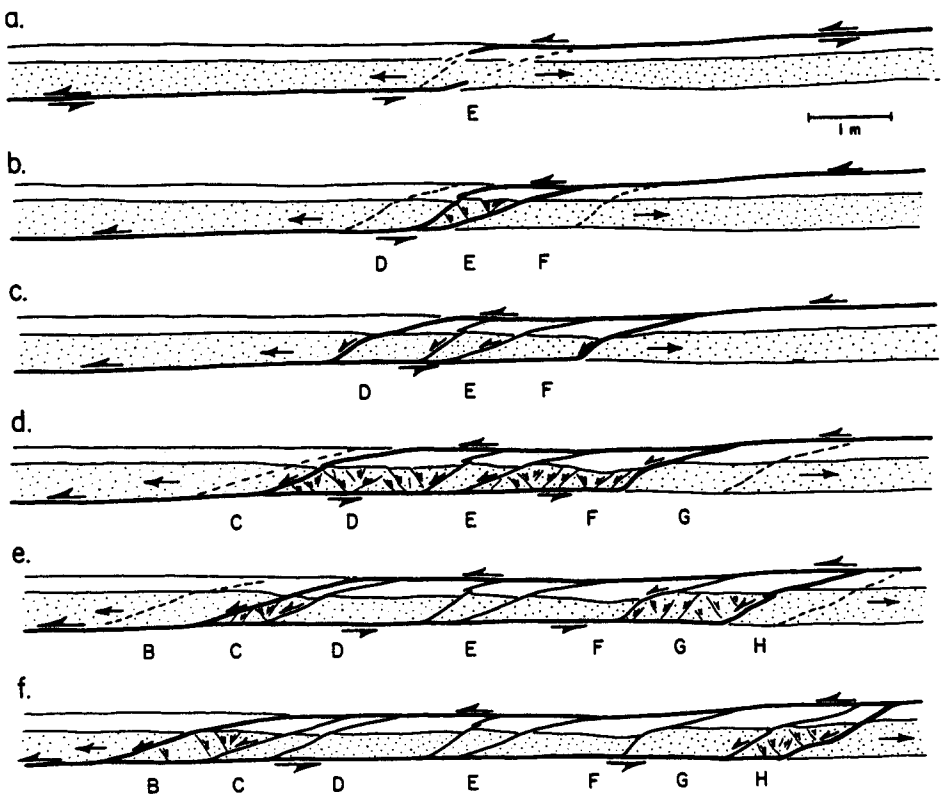

Fig. 12. Hypothesized initial en échelon fault array and developmental sequence for the quartzite-slab duplex in the Fig. 4(c) fault map: (a) initial offset en échelon fault segments; (b) initial tip-to-plane overlap linkage isolates zone E; (c)–(f) outward growth of the duplex by paired *R*-shear ruptures of the quartzite-slab to form zones D–F, C–G and B–H.

development, with the older more mature lenses near the central part of the duplex structure, as hypothesized in Fig. 12.

Layer-parallel duplex growth continued by failure of the external quartzite slab with through-going *R*-shears leading to progressive segmentation. Each *R*-shear rupture of the outer host rock walls isolates yet another doubly-tapered lens and added an increment of strain to the duplex. The isolated lens, once decoupled, could then undergo additional layer-parallel extension as slip occurred concurrently along decoupling surfaces. Various cross-cutting relations between these internal fractures consistently show the *X*- or *X'*-shear fractures offsetting the earlier more central *R*- or *R'*-shear fractures. In cross-cutting *X*–*X'*-shears, the *X*-shear fracture was the youngest structure. *R*-shears are never seen cross-cutting any internal *X*–*X'*-shears. The outward layer-parallel expansion of the duplex is thought to proceed by *R*-shear ramps cutting into the outer host rock walls with internal layer-parallel extension using the *X*–*X'* conjugate shear fracture mechanism.

Cross-cutting relations in the A–B–C zone boundary area at the southwest end of the duplex reveal a detailed sequence of fault development, again suggesting outward growth of the duplex structure. The sequence in Fig. 13 begins with the development of the more internal lenses and the layer-parallel sinistral slip surface that defines the southeast boundary fault of the duplex. Displacement along this surface to the southwest develops a long, thin zone of microbreccia (as an attrition breccia zone) that shows significant thinning and layer-parallel extension estimated at 94% corresponding to 64 cm of displacement transferred through this layer.

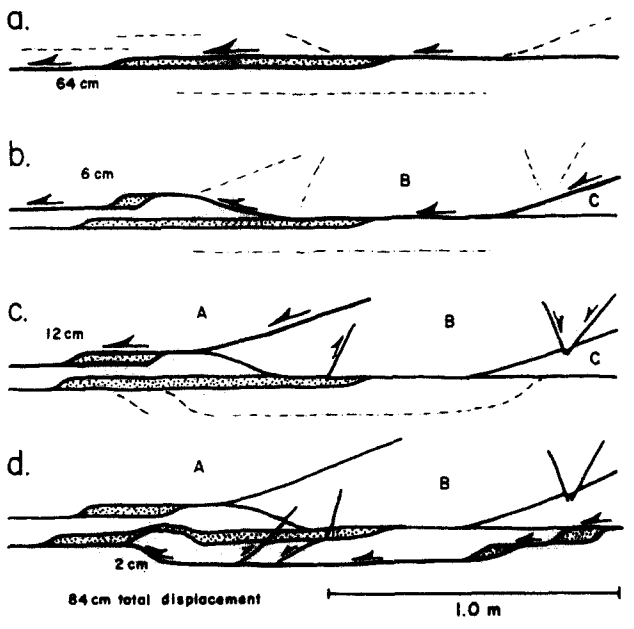

Fig. 13. Imbricate lens zone boundary sequence for the southwest end of the quartzite-slab duplex in the Fig. 4(c) fault map: (a) formation of micro-attrition-breccia by disruption of quartzite layer along left-stepping layer-parallel slip surfaces; (b) development of the B–C boundary adds displacement increment that sidesteps the earlier attrition breccia layer and creates a small dilation breccia in a left-stepping offset; (c) the formation of the A–B boundary utilizes the same structures and widens the dilation breccia zone; and (d) continued displacements accommodated along flanking surface leading to the formation of a small contractional slab and the deformation of the earlier attrition breccia layer and ramp surfaces.

Development of the *R*-shear lens boundary (C–D) led into, and through, this microbreccia zone as its last displacement increment. The *R*-shear lens boundary (B–C), on the other hand, ruptured tangentially to this zone with a small contractional ramp and a left-stepping dilational jog developing a small dilation breccia zone. The *R*-shear lens boundary (A–B) ruptured through this segment linking up to the dilation breccia zone. Further layer-parallel displacements were accommodated along a new horizon within the flanking quartzite layer. Layer-parallel extension of zone B by *X*–*X'*-shear fractures has cut down through the existing B–C boundary.

An additional increment of sinistral slip is evident in the development of the small contractional slab adjacent to this end of the segmented quartzite duplex. This structure formed with a *P*-shear ramp at the contractional end, coupled with an *R*- or *X'*-shear fracture ramp at the extensional end, defining a 1 m-long decoupled slab. The leading ramp developed a characteristic 'ramp anticline' and *P'*-shear 'backthrusts'. The deformation of the adjacent layer-parallel breccia–microbreccia unit near the crest of the ramp fold and the crosscutting relations with internal *P'*-shear back thrusts suggests that this contractional slab developed later in the sequence of structures as described above. This latest increment of displacement is most likely related to *R*-shear ruptures and duplex lens formation (zones G and H) at the northeast end of the duplex. This pattern suggests an overall symmetric growth through alternating ruptures or sequences of ruptures at either end of the quartzite-slab duplex.

DISCUSSION

The York Cliffs fault system is an excellent site to study displacement transfer across the gap or stepover zone between segmented strike-slip faults in the presence of a strong anisotropy. The duplexes result from the progressive failure of the original rock bridges between offset–overlapping en échelon fault segments upon continued displacement. An understanding of the evolution of this offset–overlap zone and the mechanism of this displacement transfer is important as it is the deformation of the stepover zone that is likely to control the slip on the main fault segments. The sense of displacement and en échelon configuration of the fault segments in these exposures create the dominantly extensional or dilational nature of the stepover zones or jog areas.

Comparison with dilational jogs

Dilational jogs are thought to play a significant role in stopping earthquake ruptures (Sibson 1985) by acting as barriers to propagation. The internal structure of the dilational jog is envisioned as a mesh of extensional fractures linked by an interconnecting shear fracture

network (Sibson 1985, 1986, Hill 1977). At York Cliffs, however, extensional fracturing played a minor role in the deformation within the dilational jog or stepover. Oblique extensional fractures are important at fault terminations, and may be an effective link between other fault segments in the exposure. In the structures studied here, however, extension in the jog areas occurred by stretching and thinning of the host rock by conjugate shear fracture mechanisms during duplex evolution rather than collapse and possible implosion of the jog under rapid dilation and decoupling. Wall rock competence appears to control the style of linkage structures with relatively rigid host rock needed to support open cavities and the formation of high dilation breccias. The progressive collapse of the stepover zone by oblique shear fracturing, or any other mechanism, likely controls slip propagation along the major fault segments. The shear fracture mechanism described above, would, most likely, have a dampening effect on slip propagation compared to a more catastrophic decoupling in the fault-parallel dilation mechanism.

Incremental or single-slip event

Cross-cutting relations indicate a progression or series of minor fault-fracture events during development of displacements along the fault system. The cumulative effect is to accommodate 1 m of displacement on the dominant layer-parallel fault segments. An important point to consider is whether this linking duplex structure represents a single earthquake event or cycle composed of minor sub-events or several earthquake events or cycles. Microtextural evidence from a very limited sampling within the fault system indicates a major cycle of brecciation and cementation suggesting a single increment of slip for those particular structures sampled at least within the time frame for growth of the cementing minerals. Some evidence can be seen in thin section for incremental development with very minor microveinlets crosscutting cementing mineralization in local dilation breccias along some faults. Most of the samples were from individual oblique faults or dilation zones so that each minor shear fracture within the linking duplex structures can be considered a single increment or component of a single event. No samples could be obtained from the dominant layer-parallel fault surfaces which most likely experienced incremental displacements.

The entire quartzite-slab duplex may have developed during a single complex event accommodating 1 m of displacement or as several *R*-shear rupture events and displacement increments. Considering the exposed fault system with horsetail termination arrays at both ends as a single fault with a length of 150 m, likely incremental displacement/length ratios can be compared with present-day earthquakes. Typical incremental displacement/length ratios for known fault ruptures range from 10^{-4} to 10^{-5} (Sibson personal communication 1989). The most likely rupture sequence in terms of displacement/length ratios, as well as kinematic development, appears to be the individual *R*-shear event model with incremental displacements on the order of 10 cm and displacement/length ratios in the 10^{-4} range.

Localized stress field variations

Cross-cutting relations and models for duplex development as described above suggest alternating sequences of *R*–*R'*- and *X*–*X'*-shear fractures. Assuming that the shear fractures are each conjugate Coulomb shear sets, the maximum principal stress directions (Fig. 14) must be constrained to lie at ~48° to the dominant slip surface bisecting *R*–*R'* and at ~85° to the dominant slip surface bisecting *X*–*X'*, neglecting effects of rotation. Changes in stress orientations and the observed cross-cutting relations indicate cyclic stress field variations with early *R*–*R'*-shears followed by late cross-cutting *X*–*X'*-shears. Slip along the dominant fault segments and rupture of the linking *R*-shears in response to pre-failure stress orientations (Figs. 14a & b) results in localized decoupling of the stepover zones which would effectively eliminate shear stress on the layer-parallel segments. This would in turn lead to later adjustments on *X*–*X'*-shear sets in response to these post-failure stress orientations (Fig. 14c). These adjustments would be followed by a build up of shear stress at the rigid stepover due to strain hardening effects until the next cycle of *R*-shear rupture. The quartzite-slab duplex contains approximately eight dominant linking *R*-shears along with a subordinate array of minor *R'*-shears that are commonly cross-cut by later *X*–*X'*-shears. Considering each shear fracture sequence as a separate rupture

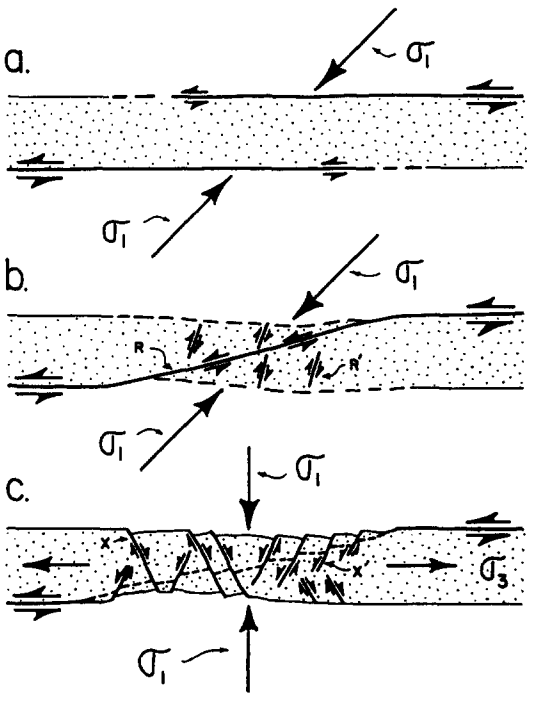

Fig. 14. Local stress configurations for a left-stepping releasing offset between sinistral strike-slip fault segments where principal stress orientations bisect sets of conjugate Coulomb shear fractures: (a) pre-failure stress orientations at offset during slip on weaker layer-parallel segments; (b) failure of intervening quartzite slab by early *R*–*R'* ruptures; and (c) post-failure stress orientations during additional fault parallel extension along late *X*–*X'* ruptures.

event, such cyclic R–R':X–X'-shear fracture development suggests, perhaps, eight stress cycles corresponding to eight R-shear rupture events with incremental displacements on the order of 10 cm. However, it is possible that this R-shear rupture sequence could have occurred within a single, albeit complex, slip event.

Effect of anisotropy

Host rock anisotropy is a key factor controlling the nature of the deformation mechanisms in these exposures. The vertical layer-anisotropy exerts a strong control on the orientation of the major fault segments, localized stress orientations and the style of deformation in the en échelon stepover. Because of the influence of this anisotropy on stress orientations, it is unclear as to the nature of the regional stress field associated with faulting. An important effect of the anisotropy here is to enhance lateral shear-fracture propagation during growth of en échelon rupture surfaces. This lateral propagation along the anisotropy promotes tip-to-plane linkages between overlapping en échelon segments rather than tip-to-tip linkages. This leads to the development of extensional duplexes in the overlap zones rather than localized high dilation jogs between offset fracture tips. The elongate overlap zones and slab duplexes develop where fault segments step across competent layers or zones in the anisotropic host rocks.

Implications for earthquake generation

The evidence presented above suggests the development of incremental slip along this fault with successive stress cycles represented by the R-shear rupture:X–X' extension sequences in the episodic growth of the duplex. The X–X'-shear fracturing may reflect an accelerated phase of post-seismic creep. It is likely that the failure of this offset–overlap zone controls slip on the main fault segments and that the increment of slip is controlled by the specific deformation mechanism for the quartzite slab. In extensional and contractional stepover zones where duplexing is developed this deformation involves progressive imbrication. In the York Cliffs example, the specific deformation mechanism for extensional imbrication is the R-shear rupture of the quartzite slab. The anisotropy in the host rocks in this example enhances episodic imbrication of the quartzite slabs and the development of elongated duplexes along the anisotropy. This repeatable R-shear rupture mechanism would assure a sequence of similar earthquake ruptures associated with the episodic growth of the duplex accommodation zone. There still remains the possibility that the R-shear rupture sequences developed during the same earthquake event as a cascade of failure allowing a single increment of displacement along the fault system.

The displacement–length profile (Fig. 15) is distinctly asymmetric reflecting differences in strain accommodation in the host rocks along strike adjacent to the fault. The asymmetric profile is interpreted as a composite of

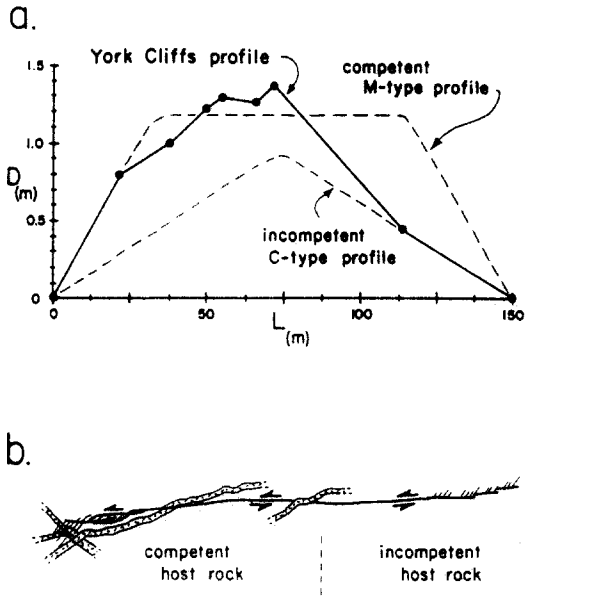

Fig. 15. (a) Displacement–length profile for York Cliffs fault system where the M (or mesa) type and C (or cone) type profiles follow Muraoka & Kamata (1983); (b) asymmetric profile attributed to the distribution of competent (larger dikes, quartzite layers and fold hinge zone) and incompetent (layer-parallel segments in pelitic layers) host rocks along the length of the fault.

the M-type profile, after Muraoka & Kamata (1983), for competent host rock and the C-type profile for incompetent host rocks. Host rock at the northeast end of the fault is considered incompetent where the fault runs largely layer-parallel concentrating strain in the weaker pelitic beds. The host rock at the southwest end of the fault is considered competent where the fault has stepped across thicker quartzite beds, an F_2 hinge zone and several larger Mesozoic dikes.

The York Cliffs fault system can best be modelled as a series of layer-parallel fault segments whose ends are offset across competent upright quartzite beds. The layer-parallel segments are essentially weak, as strain is localized in the pelitic units that flank the intervening quartzite slabs. The offset–overlap zones remain as unbroken competent host rock acting as a barrier to slip on the entire fault system.

The failure model illustrated in Fig. 16 portrays fault slip as a sequence of R-shear ruptures of the intervening quartzite slab. Each R-shear rupture induces slip along the weaker layer-parallel segments so that slip propagation extends outwards in both directions, expanding the slip surface to full fault dimensions. Rupture propagation to the terminations would also build the tensional fractures in the horsetail termination arrays. Successive ruptures or events would be possible due to geometric strain hardening of the R-shears at the stepover and/or cementation by calcite–quartz mineralization. By analogy to larger-scale faults and earthquakes, these structures would represent a pattern of focal rupture and outward slip propagation. The focus was initially defined as a barrier to slip propagation as the unbroken en échelon offset zone, but later evolves as an asperity whose sequential rupture controls slip on the entire fault system.

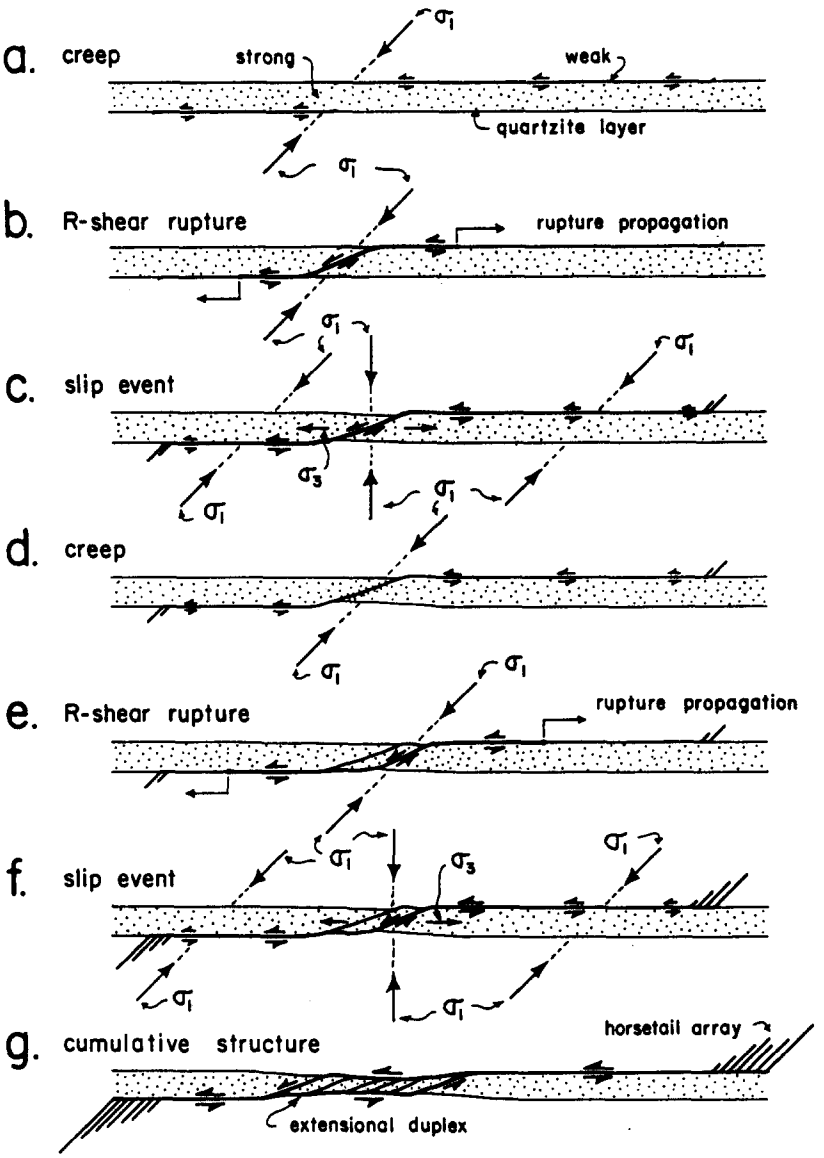

Fig. 16. Failure sequence for York Cliffs fault system modeled as weak layer-parallel fault segments in pelitic host rocks and a strong en échelon offset where fault steps across rigid quartzite layers: (a) creep along weak fault segments builds stress at en échelon offset; (b) *R*-shear rupture of rigid quartzite layer induces slip propagation along adjoining weaker layer-parallel segments; (c) slip event or increment as rupture and slip expand to full fault dimensions with the development of oblique tension fractures in horsetail array at termination; (d) creep phase renewed with locking of ruptured quartzite layer due to geometric strain hardening and/or cementation that rebuilds stresses at en échelon offset; (e) *R*-shear rupture of rigid quartzite layer begins building duplex and induces slip propagation along adjoining weaker layer-parallel fault segments; (f) slip event or increment as rupture and slip expand to full fault dimensions leading to development of the horsetail termination array; and (g) cumulative structure after multiple slip events as extensional duplex.

CONCLUSIONS

Duplex development in strike-slip faults may be an effective mechanism for accommodating strain across the offset–overlap zones between en échelon fault segments without the formation of significant open-cavity mineralization and dilation breccia. An elongate slab geometry is enhanced by any pre-existing planar, fault-parallel anisotropy in the host rocks. In the Kittery Formation at York Cliffs the vertical bedding-anisotropy strongly controls the geometry of rupture between the left-stepping en échelon sinistral strike-slip fault segments. Offset–overlapping fault segments develop linking structures at the stepover zones that form long duplexes along competent quartzite layers. The internal shear fracture deformation of these quartzite slabs plays a significant role in accommodating displacements along the fault structure. Increased displacements are accommodated by growth of the extensional duplex through *R*-shear segmentation. The duplexes can accommodate nearly 10% total layer-parallel extension and as much as 14% locally without significant brecciation utilizing *R*-shear segmentation and *X*–*X*′ conjugate shear fracture mechanisms for distributing the strain.

Acknowledgements—Research for this project was supported by the U.S. Geological Survey, Department of the Interior under the National Earthquake Hazards Reduction Program, Award Number 14-08-0001-G1395. Released time from academic duties in support of this project was provided by the University of Southern Maine. Special thanks to Rick Sibson, Dave Sanderson and an anonymous reviewer for their constructive comments which greatly improved the manuscript.

REFERENCES

Boyer, S. E. & Elliot, D. 1982. Thrust systems. *Bull. Am. Ass. Petrol. Geol.* **66**, 239–267.

Dahlstrom, C. D. A. 1970. Structural geology in the eastern margin of the Canadian Rocky Mountains. *Bull. Can. Petrol. Geol.* **18**, 332–406.

Doherty, J. T. & Lyons, J. B. 1980. Mesozoic erosion rates in northern New England. *Bull. geol. Soc. Am.* **91**, 16–20.

Engelder, J. T. 1974. Cataclasis and the generation of fault gouge. *Bull. geol. Soc. Am.* **85**, 1515–1522.

Friedman, M. & Logan, J. M. 1970. Microscopic feather fractures. *Bull. geol. Soc. Am.* **11**, 3417–3420.

Gibbs, A. D. 1984. Structural evolution of extensional basin margins. *J. geol. Soc. Lond.* **141**, 609–620.

Granier, T. 1985. Origin, damping and pattern of development of faults in granite. *Tectonics* **4**, 721–737.

Hanmer, S. 1989. Initiation of cataclastic flow in a mylonite zone. *J. Struct. Geol.* **11**, 751–762.

Hempton, M. R. & Neher, K. 1986. Experimental fracture, strain and subsidence patterns over en échelon strike-slip faults: implications for the structural evolution of pull-apart basins. *J. Struct. Geol.* **8**, 597–605.

Hill, D. P. 1977. A model for earthquake swarms. *J. geophys. Res.* **82**, 1347–1352.

Hussey, A. M. 1962. The geology of southern York County, Maine. *Bull. Maine geol. Surv.* **4**, 1–67.

Logan, J. M., Friedman, M., Higgs, N., Dengo, C. & Shimamoto, T. 1979. Experimental studies of simulated gouge and their application to studies of natural fault zones. *U.S. geol. Surv. Open-File Rep.* **79-1239**, 305–343.

Muraoka, H. & Kamata, H. 1983. Displacement distribution along minor fault traces. *J. Struct. Geol.* **5**, 483–495.

Sibson, R. H. 1983. Continental fault structure and the shallow earthquake source. *J. geol. Soc. Lond.* **140**, 741–767.

Sibson, R. H. 1985. Stopping of earthquake ruptures at dilational fault jogs. *Nature* **316**, 248–251.

Sibson, R. H. 1986. Brecciation processes in fault zones: inferences from earthquake rupturing. *Pure & Appl. Geophys.* **124**, 159–175.

Swanson, M. T. 1982. The structure and tectonics of Mesozoic dike swarms in eastern New England. Unpublished Ph.D. dissertation, State University of New York at Albany.

Swanson, M. T. 1987. Strike-slip duplex structures in vertical anisotropic rocks. *Geol. Soc. Am. Abs. w. Prog.* **19**, 861.

Swanson, M. T. 1988. Pseudotachylyte-bearing strike-slip duplex structures in the Fort Foster Brittle Zone, S. Maine. *J. Struct. Geol.* **10**, 813–828.

Swanson, M. T. 1989. Sidewall ripouts in strike-slip faults. *J. Struct. Geol.* **11**, 933–948.

Woodcock, N. H. & Fischer, M. 1986. Strike-slip duplexes. *J. Struct. Geol.* **8**, 725–735.